Defence Research and Development Canada | Recherche et développement pour la défense Canada

CAN UNCLASSIFIED

DRDC | RDDC
technologysciencetechnologie

Active Turbulent Imaging Simulation on Weak Specular Targets

Guy Potvin
DRDC – Valcartier Research Centre

8th International Symposium on Optronics In Defence and Security, OPTRO2018, 6–8 February 2018, Paris, France

Date of Publication from Ext Publisher: February 2018

Defence Research and Development Canada
External Literature (N)
DRDC-RDDC-2018-N007
February 2018

Canada

IMPORTANT INFORMATIVE STATEMENTS

This document was reviewed for Controlled Goods by Defence Research and Development Canada (DRDC) using the Schedule to the *Defence Production Act*.

ACTIVE TURBULENT IMAGING SIMULATION ON WEAK SPECULAR TARGETS

OECD CONFERENCE CENTER, PARIS, FRANCE / 6 – 8 FEBRUARY 2018

Guy Potvin

DRDC – Valcartier Research Centre, 2459 de la Bravoure Road, Québec, QC, G3J 1X5, Canada
Email:guy.potvin@drdc-rddc.gc.ca

KEYWORDS: Simulation, turbulence, propagation, Wigner function, BRDF

ABSTRACT:

We define the *Bidirectional Reflectivity Distribution Function* (BRDF) in terms of Wigner functions so as to make its radiometric aspect compatible with the wave aspect of coherent propagation through atmospheric turbulence. We then adapt this definition in order to make it compatible with the DRDC turbulent imaging simulator for active imaging on weakly specular surfaces. This is done by defining a coherence length associated with the surface which expresses how specular it is. We demonstrate our model on a few targets and comment on its range of applicability.

1. INTRODUCTION

The *Bidirectional Reflectivity Distribution Function* (BRDF) describes how the surface of an object absorbs radiance coming from a given direction and radiates it into another [1]. As such, it plays an important role in the simulation of active imaging systems. However, it was defined in the context of radiometry, where objects emit radiation incoherently and which radiates in straight lines. This picture is incompatible with electromagnetic waves propagating through atmospheric turbulence from a coherent source such as a laser.

We attempt to make turbulent coherent propagation and the BRDF compatible by using Wigner transforms [2], which turns the *Mutual Coherence Function* (MCF) of the electromagnetic field into a quasi-probability distribution in phase space (position and momentum). This Wigner function is real, has the correct marginal distributions and the momentum coordinate can be interpreted as the direction of a ray. However, the Wigner function can also be negative in places, or be non-zero in places where we know there shouldn't be any electromagnetic energy [3]. Nevertheless, the Wigner function can be very useful in optics and imaging systems [4-7].

In this work, we will briefly review the Wigner function and its propagation through turbulence in Sec. 2. We then define the BRDF in terms of Wigner functions and show how the BRDF changes an incident Wigner function on a surface into a scattered Wigner function in Sec. 3. We apply this theory to our turbulent imaging simulator [8, 9] for active imaging by using the paraxial approximation in Sec. 4. This leads us to define a coherence length for the surface which quantifies how specular it is. We show how to model weakly specular surfaces seen through turbulence in Sec. 5. We also show some outputs of our model on a few simple targets in Sec. 5 and comment on its range of applicability in the conclusion in Sec. 6.

2. THEORETICAL PRELIMINARIES

In this section, we will define the Wigner function and show how it propagates through the atmosphere.

2.1. The Wigner function

For *Electro-Optic* (EO) propagation through the atmosphere in the visible and IR bands, the electric field can be treated as a complex scalar without loss of generality: $E(\vec{x},t)$. We can define a quasi-probability function in phase space as:

$$W(\vec{R},T,\vec{P},\mathbb{E}) = \left(\frac{1}{2\pi\hbar}\right)^4 \int \mathrm{d}^3\,\Delta \int \mathrm{d}\,\tau \times \exp\left[i\left(\mathbb{E}\tau - \vec{P}\cdot\vec{\Delta}\right)/\hbar\right] \Gamma(\vec{R},\vec{\Delta},T,\tau), \quad (1)$$

where $\vec{R}$ and T are a central position and time respectively, and where $\vec{P}$ and $\mathbb{E}$ are the corresponding momentum and energy. Also, the MCF in Eq. 1 is:

$$\Gamma(\vec{R},\vec{\Delta},T,\tau) = \langle E\left(\vec{R}+\vec{\Delta}/2\,,T+\tau/2\right) \times E^*\left(\vec{R}-\vec{\Delta}/2\,,T-\tau/2\right)\rangle, \quad (2)$$

where the angle brackets represent the average over a suitable ensemble. This could be the ensemble of turbulent fluctuations, the random microscopic fluctuations of a reflecting surface or no ensemble at all. The inverse of Eq 1 is:

$$\Gamma(\vec{R},\vec{\Delta},T,\tau) = \int \mathrm{d}^3\,P \int \mathrm{d}\,\mathbb{E} \times \exp\left[i\left(\vec{P}\cdot\vec{\Delta} - \mathbb{E}\tau\right)/\hbar\right]\; W(\vec{R},T,\vec{P},\mathbb{E})\,. \quad (3)$$

2.2. Atmospheric propagation

For *EO* propagation, the wave equation for the

electric field is:

$$\nabla^2 E - \frac{n^2}{c^2}\frac{\partial^2 E}{\partial t^2} \approx 0\,, \tag{4}$$

where n is the turbulent refractive index of the atmosphere. If we assume that the refractive index changes over a timescale much longer than the period of the electric field, then we can approximate it as: $E \approx u\exp[-i\hbar\omega]$, where ω is the angular frequency of the radiation and u changes very slowly with respect to the period.

Under these conditions, the Wigner function defined in Eq. 1 will very sharply peaked about the energy, $\mathbb{E} = \hbar\omega$. We can define a new Wigner function by integrating Eq. 1 with respect to energy, giving us the expression:

$$W(\vec{R},T,\vec{P}) = \left(\frac{1}{2\pi\hbar}\right)^3 \int \mathrm{d}^3\,\Delta \exp\left[-i\vec{P}\cdot\frac{\vec{\Delta}}{\hbar}\right] \times u\left(\vec{R}+\vec{\Delta}/2\,,T\right)u^*\left(\vec{R}-\vec{\Delta}/2\,,T\right). \tag{5}$$

From Eq. 4, it is possible to show that the Wigner function from Eq. 5 approximately obeys the phase-space conservation equation:

$$\frac{\partial}{\partial T}\left(\frac{\hbar\omega n^2}{c^2}W\right) + \vec{\nabla}_R\cdot\left(W\vec{P}\right) + \frac{\vec{\nabla}_R n}{n}\cdot\vec{\nabla}_P\left(\left(\frac{\hbar\omega n}{c}\right)^2 W\right) \approx 0, \tag{6}$$

where $\vec{\nabla}_R$ and $\vec{\nabla}_P$ are the gradients with respect to the central position and the momentum, respectively. Note that in Eq. 6 we neglected third and higher order derivative terms with respect to the momentum. Integrating Eq. 6 with respect to $\vec{P}$ creates an energy conservation equation:

$$\frac{\partial U}{\partial T} + \vec{\nabla}_R\cdot\vec{S} = 0, \tag{7}$$

where U is the energy density:

$$U(\vec{R},T) = \int \mathrm{d}^3 P\left(\frac{\hbar\omega n^2}{c^2}\right)W(\vec{R},T,\vec{P}), \tag{8}$$

and $\vec{S}$ is the energy flux:

$$\vec{S}(\vec{R},T) = \int \mathrm{d}^3 P\, W(\vec{R},T,\vec{P})\vec{P}. \tag{9}$$

It is this quantity that will serve to define the radiance in terms of Wigner functions.

3. THE BRDF

In this section we will review the definition of the BRDF, and then show how it can be defined in terms of Wigner functions.

3.1. The definition of the BRDF

Nicodemus defined the BRDF in terms of radiance [1], which he defined as the amount of electromagnetic energy going through a surface from a given direction per unit time, per unit solid angle, per unit area perpendicular to the direction. Nicodemus denotes radiance with a scalar function N with units of Watts per area per steradians, such that:

$$N = \frac{\partial P}{\cos\theta\,\partial\Omega\partial A}, \tag{10}$$

where ∂P, $\partial\Omega$ and ∂A are increments of power, solid angle and area respectively, and θ is the angle between the normal of the surface and the direction of the radiance.

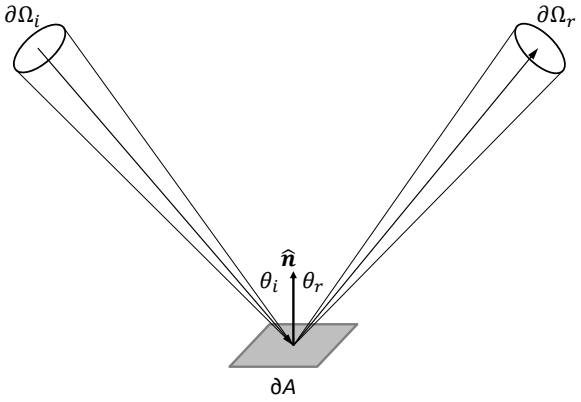

Figure 1. Illustration of the BRDF definition.

Fig. 1 illustrates the physical situation defining the BRDF. On the left there is the incoming radiance N_i on the surface increment ∂A. This radiance comes from a solid angle increment $\partial\Omega_i$ centred about the direction (solid black arrow) $\vec{\Omega}_i = (\phi_i,\theta_i)$, where θ_i is the angle with respect to the surface normal $\hat{n}$ and ϕ_i is the angle in the surface plane (not shown). The surface increment then emits radiance N_r in the solid angle increment $\partial\Omega_r$ centred about the direction $\vec{\Omega}_r = (\phi_r,\theta_r)$. The BRDF relates the radiances at the point $\vec{\rho}_s$ on the surface in the following way:

$$N_r(\vec{\rho}_s,\vec{\Omega}_r) = \int_h \mathrm{d}\,\Omega_i\, N_i(\vec{\rho}_s,\vec{\Omega}_i)\cos\theta_i \times \sigma(\vec{\rho}_s,\vec{\Omega}_i;\vec{\Omega}_r), \tag{11}$$

where σ is the BRDF (with units of inverse steradians) and the subscript h beneath the integral signifies that the integration is limited to the hemisphere above the surface. Note that the cosine in the integrand of Eq. 11 means that only the incoming radiance that passes through the surface contributes to the emitted radiance.

3.2. Definition using Wigner functions

We postulate the following definition of radiance in terms of the Wigner function:

$$N(\vec{R},\hat{P}) = \int_0^\infty \mathrm{d}\,P\,P^3 W(\vec{R},P,\hat{P}), \tag{12}$$

where we explicitly decompose the momentum vector $\vec{P}$ into its magnitude P and its unit vector $\hat{P}$, which encodes information about direction. We also assume that we have a time-independent steady-state. From our definition of the energy flux in Eq. 9, it is easy to see that:

$$\vec{S}(\vec{R}) = \int \mathrm{d}\,\Omega\,\hat{P}\,N(\vec{R},\hat{P}), \tag{13}$$

where the integration is over the entire sphere. Equation 13 is the relation we expect between radiance and energy flux. We now relate the emitted Wigner function with the incident Wigner function using a reflectance function Σ at the surface such that:

$$W_r(\vec{\rho}_s,\vec{P}_r) = \int \mathrm{d}^3\,P_i\,W_i(\vec{\rho}_s,\vec{P}_i)\Sigma(\vec{\rho}_s,\vec{P}_i;\vec{P}_r). \tag{14}$$

We obtain a model that conforms to Eq. 11 if we postulate the following:

$$\Sigma(\vec{\rho}_s,\vec{P}_i;\vec{P}_r) = -\left(\frac{\hat{P}_i\cdot\hat{n}}{P_r^2}\right)\delta(P_r-P_i) \times \sigma(\vec{\rho}_s,\hat{P}_i,\hat{n};\hat{P}_r). \tag{15}$$

The minus sign on the right-hand side of Eq. 15 is there to compensate for the fact that the inner product $\hat{P}_i\cdot\hat{n}$ is negative, since the incoming ray forms an angle greater than 90 degrees with respect to the normal of the surface $\hat{n}$ as shown in Fig. 1. Placing the reflectance function in Eq. 15 in Eq. 14 gives us:

$$W_r(\vec{\rho}_s,P_r,\hat{P}_r) = \int \mathrm{d}\,\Omega_i\,W_i(\vec{\rho}_s,P_r,\hat{P}_i)\cos\theta_i \times \sigma(\vec{\rho}_s,\hat{P}_i,\hat{n};\hat{P}_r). \tag{16}$$

If we multiply both sides of Eq. 16 by P_r^3 and integrate, it is easy to see with the definition of radiance in Eq. 12 that we obtain the desired result in Eq. 11.

4. THE ACTIVE IMAGING MODEL

Having defined the BRDF in terms of Wigner functions, we are now ready to implement it in an active imaging model through the atmosphere. This model is illustrated in Fig. 2, where a laser emits a ray towards the target surface a distance L away. The ray travels through turbulence and gets deviated, it then is reflected off the target surface and returns to the imager, going through the turbulence a second time.

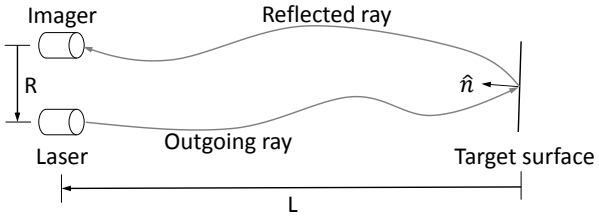

Figure 2. Illustration of active imaging through atmospheric turbulence.

Since the range of the target is typically much larger than the distance separating the laser from the imager, the incident and reflected rays are always very nearly parallel to the line-of-sight of the active imaging system (which we take to be the *z*-axis in our system of coordinates). We therefore begin by reviewing the paraxial approximation for propagation and the Wigner function. We then examine the simplifications that obtain for the BRDF in this limit.

4.1. The paraxial propagation

Since we assume a steady-state, the function u obeys the equation:

$$\nabla^2 u + k_0^2 n^2 u = 0\,, \tag{17}$$

where $k_0 = \omega/c$ is the nominal wavenumber for empty space. We also assume the u propagates mainly along the *z*-axis so that $u = a\exp[ik_0 z]$. If we further assume that the refractive index has small turbulent fluctuations, such that $n = 1 + n_1$ where $n_1 \ll 1$, we obtain the equation for a:

$$\nabla_\rho^2 a + \partial_z^2 a + 2ik_0\partial_z a + 2k_0^2 n_1 a \approx 0\,, \tag{18}$$

where $\partial_z = \partial/\partial z$ is the partial derivative with respect to the *z*-coordinate and $\vec{\nabla}_\rho$ is the gradient with along the *x*-*y* plane $\vec{\rho} = (x,y)$. Finally, we assume that the function a varies slowly along the *z*-axis with respect to the wavelength, so that $|\partial_z^2 a| \ll |2k_0\partial_z a|$ and we get:

$$i\partial_z a + \frac{1}{2k_0}\nabla_\rho^2 a + k_0 n_1 a \approx 0\,, \tag{19}$$

which is the paraxial propagation equation. Using these assumptions in the Wigner function definition Eq. 5 leads to:

$$W(\vec{R},\vec{P}) \approx \frac{\delta(P_z-\hbar k_0)}{(\hbar k_0)^2}\widetilde{W}(\vec{R},\vec{p}), \tag{20}$$

where:

$$\widetilde{W}(\vec{R},\vec{p}) = \left(\frac{k_0}{2\pi}\right)^2 \int \mathrm{d}^2 D \exp\left[-ik_0\vec{p}\cdot\vec{D}\right] \times a\left(\vec{C}+\vec{D}/2, Z\right)a^*\left(\vec{C}-\vec{D}/2, Z\right). \quad (21)$$

In Eqs. 20 and 21 we used the notation $\vec{R} = (\vec{C}, Z)$, where $\vec{C}$ is the central position along the *x*-*y* plane and Z is the central position along the *z*-axis. We also used the notation $\vec{P} = (\vec{P}_c, P_z)$, where $\vec{P}_c$ is the momentum conjugate to the $\vec{C}$ coordinate and P_z is conjugate to the Z coordinate. The momentum in Eq. 21 is $\vec{p} = \vec{P}_c/(\hbar k_0)$, which is dimensionless and approximately equals the slope of the ray trajectory. The phase-space conservation equation for $\widetilde{W}$ is approximately:

$$\partial_Z \widetilde{W} + \vec{\nabla}_C \cdot \left(\widetilde{W}\vec{p}\right) + \vec{\nabla}_C n_1 \cdot \vec{\nabla}_p \widetilde{W} \approx 0. \quad (22)$$

4.2. The paraxial BRDF

We wish to model the BRDF as a more or less diffuse reflection, such as shown in Fig. 3 where the incident ray (grey arrow) produces a reflected ray (red arrow) along with scattered rays (blue arrows) distributed about the reflected ray.

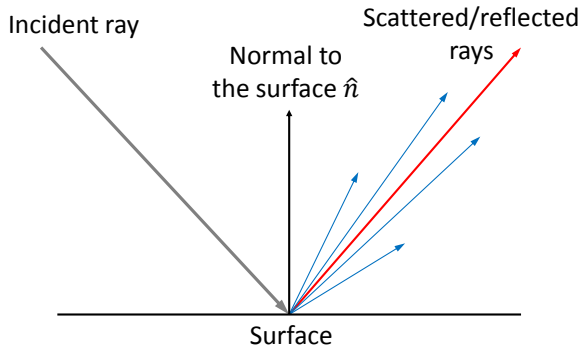

Figure 3. The diffuse reflection

The reflected ray unit vector $\hat{P}_0$ obeys the relation:

$$\hat{P}_0 = \hat{P}_i - 2\left(\hat{P}_i \cdot \hat{n}\right)\hat{n}, \quad (23)$$

where $\hat{n}$ is the normal of the reflecting surface. We model the target surface as a function:

$$Z_s = f\left(\vec{C}_s\right), \quad (24)$$

where Z_s is the *z*-coordinate of the surface as a function of the *x*-*y* coordinates of the target plane $\vec{C}_s$. The gradient of the target surface is:

$$\vec{g} = \vec{\nabla}_C f, \quad (25)$$

and the surface normal unit vector is:

$$\hat{n} = \frac{(-\vec{g}, 1)}{\sqrt{1+g^2}}. \quad (26)$$

Likewise, the unit reflected and incident momenta vectors are:

$$\hat{P}_0 = \frac{(\vec{p}_0, 1)}{\sqrt{1+p_0^2}}, \quad \hat{P}_i = -\frac{(\vec{p}_i, 1)}{\sqrt{1+p_i^2}}. \quad (27)$$

Since we want the paraxial approximation, the incident ray should be very nearly parallel to the z-axis and so its slope should be very small: $p_i \ll 1$. Also assuming that the target surface gradient is small, $g \ll 1$, Eq. 23 becomes:

$$\vec{p}_0 \approx -\vec{p}_i - 2\vec{g}, \quad (28)$$

since $\hat{P}_i \cdot \hat{n} \approx -1$. Furthermore, in the paraxial limit the *z*-component of the momenta are almost equal to their magnitude, such that $P_{rz} \approx P_r \approx \hbar k_0$ and $P_{iz} \approx -P_i \approx -\hbar k_0$. Therefore, placing Eq. 15 and Eq. 20 in Eq. 14 and using all of the approximations mentioned in this section and integrating with respect to the momenta z-components, we obtain:

$$\widetilde{W}_r(\vec{C}_s, \vec{p}_r) = \int \mathrm{d}^2 p_i \, \widetilde{W}_i(\vec{C}_s, \vec{p}_i)\sigma(\vec{C}_s, \vec{p}_i, \vec{g}; \vec{p}_r), \quad (29)$$

where we use a Gaussian approximation for the BRDF:

$$\sigma(\vec{C}_s, \vec{p}_i, \vec{g}; \vec{p}_r) = \alpha(\vec{C}_s) \times \frac{k_0^2 l^2}{2\pi}\exp\left[-\frac{k_0^2 l^2}{2}(\vec{p}_r + \vec{p}_i + 2\vec{g})^2\right]. \quad (30)$$

In Eq. 30, the factor $\sigma(\vec{C}_s)$ is the reflectivity of the surface and is a function of position. The *coherence length* $l(\vec{C}_s)$ controls the scattering of the rays about the reflection ray and is also a function of position. A coherence length much smaller than the wavelength corresponds to a wide spread of slopes, and a length much greater than the wavelength corresponds to a very narrow spread of the slopes.

We can gain insight by considering the incident and scattered MCFs. Recalling the inversion formula in Eq. 3, we can write the equivalent of Eq. 29 for MCFs:

$$\tilde{\Gamma}_r(\vec{C}_s, \vec{D}_r) = \int \mathrm{d}^2 D_i \, \tilde{\Gamma}_i(\vec{C}_s, \vec{D}_i)\, \beta(\vec{C}_s, \vec{D}_i, \vec{g}; \vec{D}_r), \quad (31)$$

where:

$$\beta(\vec{C}_s, \vec{D}_i, \vec{g}; \vec{D}_r) = \left(\frac{k_0}{2\pi}\right)^2 \int \mathrm{d}^2 p_i \int \mathrm{d}^2 p_r \times \exp\left[ik_0\left(\vec{p}_r\cdot\vec{D}_r - \vec{p}_i\cdot\vec{D}_i\right)\right]\sigma(\vec{C}_s, \vec{p}_i, \vec{g}; \vec{p}_r), \quad (32)$$

which gives:

$$\beta(\vec{C}_s, \vec{D}_i, \vec{g}; \vec{D}_r) = \alpha(\vec{C}_s)\delta(\vec{D}_r + \vec{D}_i) \times \exp\left[-\frac{D_i^2}{2l^2} + 2ik_0\vec{D}_i \cdot \vec{g}\right]. \quad (33)$$

Placing Eq. 33 in Eq. 31 results in the simple relationship:

$$\tilde{\Gamma}_r(\vec{C}_s, \vec{D}_r) = \tilde{\Gamma}_i(\vec{C}_s, -\vec{D}_r)\alpha(\vec{C}_s) \times \exp\left[-\frac{D_r^2}{2l^2} - 2ik_0\vec{D}_r \cdot \vec{g}\right] \quad (34)$$

Equation 34 describes a simple BRDF for paraxial propagation with small target surface gradients. In it, we see that the scattered MCF has its coherence reduced by a factor $\exp[-D_r^2/(2l^2)]$. Therefore, if the coherence length is very small, then a highly coherent incident MCF (such as from a plane wave) will result in an incoherent (Lambertian) scattered MCF. Conversely, a surface with a very large coherence length will not alter the coherence of the MCF, such that an incident plane wave will result in an outgoing plane wave with a wavenumber vector corresponding to a reflection with no diffusion or scattering.

5. MODELING THE TURBULENCE

We have adapted our passive turbulent imaging simulator [8, 9] to function as an active turbulent imaging simulator based on the BRDF developed above. We begin this section with a brief review of the model's physical principles and how they interact with the BRDF, and then we show and comment on some sample outputs.

5.1. Physical principles

Our model is based on an *Extended Huygens-Fresnel* (EHF) principle (see Fante [10]). If we have the function $a_e(\vec{\rho}_e, L)$ on the emitting surface of a laser, and the want to find the corresponding incident function on the target surface $a_i(\vec{\rho}_s, 0)$ (as shown in Fig. 2), we use a propagator such that:

$$a_i(\vec{\rho}_s, 0) = \int \mathrm{d}^2\,\rho_e\; a_e(\vec{\rho}_e, L)\psi(\vec{\rho}_e, L; \vec{\rho}_s, 0), \quad (35)$$

where:

$$\psi = \frac{k_0}{2\pi i L}\exp\left[\frac{ik_0}{2L}(\vec{\rho}_s - \vec{\rho}_e)^2 + \chi + iS\right]. \quad (36)$$

The first term in the exponent of Eq. 36 corresponds to a spherical wave in empty space. The terms $\chi(\vec{\rho}_e, L; \vec{\rho}_s, 0)$ and $S(\vec{\rho}_e, L; \vec{\rho}_s, 0)$ are fluctuations caused by turbulence of the log-amplitude and phase, respectively. Note that the model uses the Rytov approximation for the log-amplitude and phase fluctuations, making them linear integrals of the refractive index fluctuation field, n_1. We will not elaborate on this here.

The equation for the MCFs corresponding to Eq. 35 is:

$$\tilde{\Gamma}_i(\vec{C}_s, \vec{D}_s, 0) = \int \mathrm{d}^2\,C_e \int \mathrm{d}^2\,D_e \tilde{\Gamma}_e(\vec{C}_e, \vec{D}_e, L) \times H(\vec{C}_e, \vec{D}_e, L; \vec{C}_s, \vec{D}_s, 0), \quad (37)$$

where:

$$H(\vec{C}_e, \vec{D}_e, L; \vec{C}_s, \vec{D}_s, 0) = \psi\left(\vec{C}_e + \frac{\vec{D}_e}{2}; \vec{C}_s + \frac{\vec{D}_s}{2}\right) \times \psi^*\left(\vec{C}_e - \frac{\vec{D}_e}{2}; \vec{C}_s - \frac{\vec{D}_s}{2}\right). \quad (38)$$

In order to find the scattered MCF, we will make two simplifications: first, we model the laser as a point source located at $\vec{C}_e$ with an infinite beam divergence, and second we assume that the coherence length is significantly shorter than the correlation scales for χ and S. This means that surface is *weakly specular* and that we can expand those fields as a Taylor series and keep the zero and first order terms. From Eq. 34 we get:

$$\tilde{\Gamma}_r(\vec{C}_s, \vec{D}_r) = \alpha(\vec{C}_s)\left(\frac{k_0}{2\pi L}\right)^2 \times \exp\left[-\frac{D_r^2}{2l^2} + 2\chi + ik_0\vec{D}_r \cdot \vec{\gamma}\right], \quad (39)$$

where:

$$\vec{\gamma} = \frac{\vec{C}_s - \vec{C}_e}{L} + \frac{1}{k_0}\vec{\nabla}_C S - 2\vec{g}. \quad (40)$$

The model then propagates the scattered MCF on the target surface to the imager through the same turbulence using Eqs. 37 and 38. Note that the model only uses the zero and first order derivatives at the target surface of the return χ and S fields.

5.2. Model outputs

We now demonstrate the model by simulating the illumination of a 'grey' panel (i.e. mid-way between completely black and completely white) through turbulence, where the panel has a variable coherence length. The model input values are listed in Tab. 1.

Table 1. Active imaging model input values

Range	2.3 km
Wavelength	4.2 μm
IFOV	3.83 μrad
Imager aperture diameter	18.36 cm
C_n^2	5 e -14 $m^{-2/3}$
Turbulence outer scale	10 m
Turbulence inner scale	6 mm

The values in Tab. 1 are all adjustable parameters of the model. It can therefore model visible or IR imaging simply by altering the wavelength. The

input IFOV stands for *Instantaneous Field Of View*, and is the angular divergence of a pixel of the imager. The input C_n^2 is the refractive index structure parameter. It is a statistical parameter quantifying the strength of the optical turbulence since it appears in the structure function of the refractive index turbulent fluctuations in the inertial range:

$$\langle\left(n_1(\vec{x}+\vec{l},t)-n_1(\vec{x},t)\right)^2\rangle = C_n^2 l^{2/3}, \qquad (41)$$

where the angle brackets represent the average over the ensemble of turbulent fluctuations. The inertial range refers to turbulent eddies that are smaller than the scale where the turbulence is produced (the outer scale) and larger than the scale where viscous dissipation dominates (the inner scale). See Kaimal & Finnigan [11] for more details.

Figure 4. The original grey panel

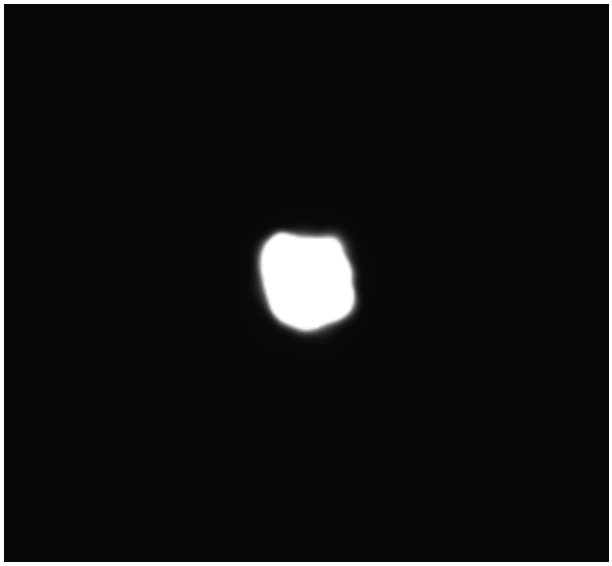

Figure 5. Model output for grey panel with a coherence length of 8 mm

Fig. 4 shows the original grey panel, whereas Fig. 5 shows the model output of the grey panel with a coherence length of 8 mm as seen by the active imaging model using the parameter input values listed in Tab. 1. Since the coherence length is very much greater than the wavelength, the surface is very specular. And since the source is collocated with the imager, only the central region returns radiance back into the imager. In the outer region, the rays reflect/scatter at angles that miss the imager entirely.

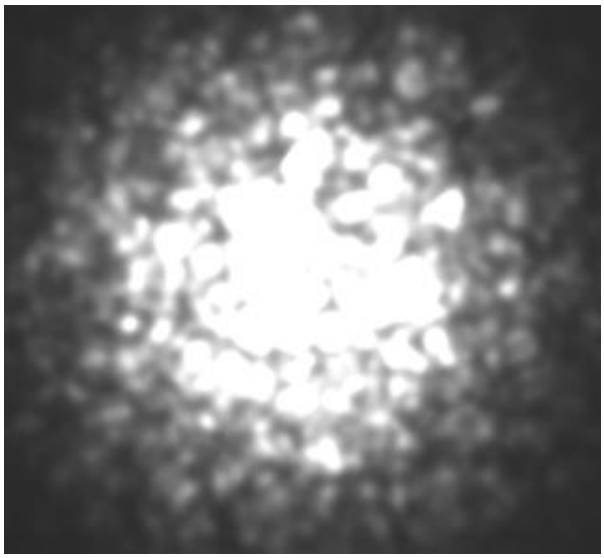

Figure 6. Model output for grey panel with a coherence length of 800 μm

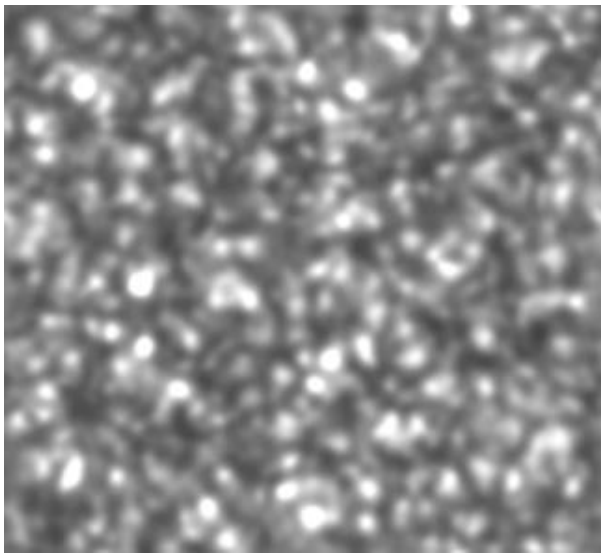

Figure 7. Model output for a Lambertian grey panel

Fig. 6 shows the same output as in Fig. 5, but with a coherence length of 800 μm. Since the coherence length is considerably shorter, the rays scatter over a wider range of angles, resulting in a greater area that returns radiance back into the imager.

Fig. 7 shows the output for a Lambertian surface, i.e. one where the coherence length is vanishingly small. That means that the rays scatter in every

direction, which results in the entire surface returning radiance to the imager. Note that the fluctuations in Fig. 7 are due entirely to the log-amplitude fluctuations, whereas those in Figs. 5 and 6 are also caused by the variable angle of arrival of the incident rays (modelled by the gradient of the function S in Eq. 40).

6. CONCLUSIONS

We have shown in this work how the BRDF of a surface can be expressed in terms of Wigner functions. This definition led to simplifications when we considered the paraxial approximation, which, in turn, led us to define the coherence length of a surface. This length describes how specular a surface is in a simple way.

However, these simplifications also come with restrictions, the most serious being the demand that the surface gradient be very small. If a scene contains objects in the foreground, it is likely that their edges will have very large surface gradients. More work is therefore needed to develop a more complete theory so as to include very large gradients.

The second most serious restriction is the demand that the surface be weakly specular so that the log-amplitude and phase fluctuation fields could be truncated to first order in a Taylor series. This means that the model would have difficulty simulating strongly specular surfaces such as the one in Fig. 5. More study is needed to determine if the distortions created by this restriction are serious and need to be addressed by modifying the model in some way.

Perhaps the least serious restriction is that the turbulence be weak enough so that the Rytov approximation holds. This restriction is a legacy from the passive turbulent imaging model on which the active model is built. It can be alleviated somewhat if the outgoing laser pulse is not modelled by the Rytov approximation (as is currently the case), but simulated by a split-step phase screen technique. However, this would still leave the problem of simulating the return propagation through strong turbulence for imaging.

Nevertheless, we believe that the coherence length concept is a simple and useful tool for modelling the active imaging of a variety of surfaces through atmospheric turbulence.

7. REFERENCES

1. Nicodemus, F. E. (1965), Directional Reflectance and Emissivity of an Opaque Surface, *Appl. Opt.*, **4**(7), 767–773.

2. Wigner, E. (1932), On the Quantum Correction for Thermodynamic Equilibrium, *Phys. Rev.*, **40**, 749–759.

3. Apresyan, L. A. and Kravtsov, Y. A. (1996), *Radiation Transfer: Statistical and Wave Aspects*, Gordon and Breach Publishers, Amsterdam NL.

4. Bastiaans, M. J. (1979), Wigner Distribution Function and its Application to First-Order Optics, *J. Opt. Soc. Am.*, **69**(12), 1710–1716.

5. Bastiaans, M. J. (1986), Application of the Wigner Distribution Function to Partially Coherent Light, *J. Opt. Soc. Am. A*, **3**(8), 1227–1238.

6. Bastiaans, M. J. and van de Mortel, P. G. J. (1996), Wigner Distribution Function of a Circular Aperture, *J. Opt. Soc. Am. A*, **13**(8), 1698–1703.

7. Alonso, M. A. (2011), Wigner Functions in Optics: Describing Beams as Ray Bundles and Pulses as Particle Ensembles, *Adv. Opt. Photonics*, **3**, 272–365.

8. Potvin, G., Forand, J. L., and Dion, D. (2007), *A Parametric Model for Simulating Turbulence Effects on Imaging Systems*, (DRDC Valcartier TR 2006-787) Defense Research and Development Canada – Valcartier.

9. Potvin, G., Forand, J. L., and Dion, D. (2011), A Simple Physical Model for Simulating Turbulent Imaging, In Holst, G. C. and Krapels, K. A., (Eds.), *Infrared Imaging Systems: Design, Analysis, Modeling and Testing XXII*, Vol. **8014** of Proc. SPIE, pp. 80140Y–13.

10. Fante, R. L. (1985), Wave Propagation in Random Media: A Systems Approach, In Wolf, E., (Ed.), *Progress in Optics*, Vol. **XXII**, 341-398, Elsevier, Amsterdam NL.

11. Kaimal, J. C., and Finnigan, J. J. (1994), *Atmospheric Boundary Layer Flows: Their Structure and Measurement*, Oxford University Press, New York.

DOCUMENT CONTROL DATA

*Security markings for the title, authors, abstract and keywords must be entered when the document is sensitive

1. ORIGINATOR (Name and address of the organization preparing the document. A DRDC Centre sponsoring a contractor's report, or tasking agency, is entered in Section 8.)

DRDC – Valcartier Research Centre
Defence Research and Development Canada
2459 route de la Bravoure
Quebec (Quebec) G3J 1X5
Canada

2a. SECURITY MARKING (Overall security marking of the document including special supplemental markings if applicable.)

CAN UNCLASSIFIED

2b. CONTROLLED GOODS

NON-CONTROLLED GOODS
DMC A

3. TITLE (The document title and sub-title as indicated on the title page.)

ACTIVE TURBULENT IMAGING SIMULATION ON WEAK SPECULAR TARGETS

4. AUTHORS (last name, followed by initials – ranks, titles, etc., not to be used)

Potvin, G.

5. DATE OF PUBLICATION (Month and year of publication of document.)	6a. NO. OF PAGES (Total pages, including Annexes, excluding DCD, covering and verso pages.)	6b. NO. OF REFS (Total references cited.)
February 2018	7	11

7. DOCUMENT CATEGORY (e.g., Scientific Report, Contract Report, Scientific Letter.)

External Literature (N)

8. SPONSORING CENTRE (The name and address of the department project office or laboratory sponsoring the research and development.)

DRDC – Valcartier Research Centre
Defence Research and Development Canada
2459 route de la Bravoure
Quebec (Quebec) G3J 1X5
Canada

9a. PROJECT OR GRANT NO. (If appropriate, the applicable research and development project or grant number under which the document was written. Please specify whether project or grant.)	9b. CONTRACT NO. (If appropriate, the applicable number under which the document was written.)

10a. DRDC PUBLICATION NUMBER (The official document number by which the document is identified by the originating activity. This number must be unique to this document.)	10b. OTHER DOCUMENT NO(s). (Any other numbers which may be assigned this document either by the originator or by the sponsor.)
DRDC-RDDC-2018-N007	

11a. FUTURE DISTRIBUTION WITHIN CANADA (Approval for further dissemination of the document. Security classification must also be considered.)

Public release

11b. FUTURE DISTRIBUTION OUTSIDE CANADA (Approval for further dissemination of the document. Security classification must also be considered.)

12. KEYWORDS, DESCRIPTORS or IDENTIFIERS (Use semi-colon as a delimiter.)

Simulation, turbulence, propagation, Wigner function, BRDF

13. ABSTRACT/RESUME (When available in the document, the French version of the abstract must be included here.)

We define the *Bidirectional Reflectivity Distribution Function* (BRDF) in terms of Wigner functions so as to make its radiometric aspect compatible with the wave aspect of coherent propagation through atmospheric turbulence. We then adapt this definition in order to make it compatible with the DRDC turbulent imaging simulator for active imaging on weakly specular surfaces. This is done by defining a coherence length associated with the surface which expresses how specular it is. We demonstrate our model on a few targets and comment on its range of applicability.